NOTES AND CORRESPONDENCE

On the Vacillation of an Unstable Baroclinic Wave Field in an Eddy-Resolving Model of the Oceanic General Circulation

WILLIAM R. HOLLAND

National Center for Atmospheric Research, Boulder, CO 80307

DALE B. HAIDVOGEL

Woods Hole Oceanographic Institution, Woods Hole, MA 02543

5 November 1980 and 9 January 1981

ABSTRACT

The vacillation of baroclinically unstable waves in a two-layer eddy-resolving oceanic circulation model is described. The vacillation cycle is distinguished kinematically by the mutual coexistence at equilibrium of short (60-day) period mesoscale eddies and a well-defined long (480-day) period modulation to the larger scale flow, as well as the long-term mean ocean circulation. Global energy budgets and related linear stability analyses reveal underlying systematic energy transfers between the slowly varying mean and transient fields of motion. The vacillation phenomenon is shown to occur over a rather narrow range of the nondimensional model parameters. Since the vacillation occurs in the presence of β, a highly structured mean flow field and meridional boundaries, this is perhaps the most complicated geophysical flow situation in which a vacillation cycle has been clearly observed.

1. Introduction

Interest in vacillation phenomena has a long history, particularly in the context of laboratory and atmospheric modeling. The heated annulus experiments of Hide (1953) were among the first to discover waves which underwent regular periodic changes in amplitude and shape, in addition to their progression. More recently, Pfeffer *et al.* (1974) and Hart (1976) have documented the synoptic and energetic character of wave vacillation in rotating fluid systems exhibiting baroclinic instability. Both studies indicate that, in addition to steady and aperiodic wave motions, various forms of frequency, wavenumber and amplitude modulation of the baroclinic wave field can occur. In the cases in which it has been sufficiently well measured, the transition from steady to wavelike flow is in accord with the predictions of linear stability theory. Experimental evidence also suggests that the observed wave modulations are related to periodic transfers of energy between the wave field and the (appropriately defined) steady circulation.

Several theoretical attempts have been made to deduce the dynamical origins of the vacillation cycles observed in these laboratory experiments. Most such studies have adopted the two-layer quasi-geostrophic equations, and either an infinite channel or a cylindrical region on an f-plane. Lorenz (1963) investigated the mechanics of vacillation in such an infinite channel model by including only disturbances of a single along-channel wavenumber and two cross-channel mode numbers. The resulting highly truncated set of ordinary differential equations were shown to yield solutions exhibiting vacillation of the baroclinic wave field, as well as steady zonal and steady wave motions. On the basis of these results, Lorenz identified at least four distinct regimes of flow: 1) a steady (and in his case symmetric) regime; 2) a steady wave regime; 3) a vacillating wave regime; and 4) an irregular, aperiodic or turbulent wave regime. Where vacillating solutions were found, steady wave solutions also appeared to exist; Lorenz further speculated that vacillating solutions may be mathematically possible in the irregular flow regime, although they are unstable.

In a similar, though less highly truncated, two-layer quasi-geostrophic model in a cylindrical f-plane region, Hart (1976) simulated the transition of steady equilibrated baroclinic waves to a baroclinic wave field with periodic modulation in amplitude and shape. The resulting model predictions of steady wave amplitudes and the occurrence of stable amplitude vacillation are in rough agreement

0022-3670/81/040557-12$07.00

with his laboratory findings (Hart, 1972). Further, the energetics of the computed limit-cycle oscillations suggest that the observed wave modulation is related to preferential and periodic energy exchanges between the steady zonal and wave flows. For his calculations, Hart concludes that baroclinic energy exchanges are dominant; barotropic processes appear to play a lesser role, though they are closely related to the changes in shape undergone by the vacillating baroclinic wave field.

Near neutral stability of the steady wave regime and for small dissipation, analytic investigations of long-period modulations of a finite-amplitude baroclinic wave are possible. In one such study, Pedlosky (1972) showed that a single wave—i.e., one having single cross-channel and along-channel wavenumbers—can only equilibrate to a steady finite amplitude if dissipation (in this case, bottom friction) is sufficiently large. For small dissipation, the steady wave regime, though theoretically possible, appears to be always unstable to finite-amplitude disturbances. As a result, unless the system is initially close to the steady solution, a limit cycle will be reached even if the steady wave solution is stable to infinitesimal perturbations. On the basis of these results, Pedlosky suggests that long-term modulations of baroclinic waves may be a natural asymptotic state of a baroclinically unstable flow, providing dissipation is sufficiently small.

These, and related studies, indicate that many geophysical systems—including annulus and dishpan experiments, limited component integrations of the quasi-geostrophic equations, and analytic single wave solutions near neutral stability—exhibit vacillation phenomena. Despite a possible application to observed index cycles in the atmosphere (Webster and Keller, 1975), however, the existence of similar phenomena in more complicated geophysical systems is uncertain. Not only do existing laboratory, numerical and analytic models omit physical and geometric influences such as β, spatial inhomogeneities in the mean flow and meridional boundaries (all of which may be important to the detailed mechanics of vacillation cycles), but specific examples of vacillation in the presence of these complicating factors have not been documented.

In this note, we briefly describe a vacillation of unstable baroclinic waves which has been observed in an eddy-resolving ocean circulation model (EGCM). Although instances of steady, regular (simple) wavelike and irregular (turbulent) motions have all been documented in recent EGCM parameter studies (e.g., Holland, 1978), the experiments to be described appear to be the first in which a well-defined vacillation cycle has also been observed. The vacillation occurs in the presence of β, a spatially highly inhomogeneous flow and meridional boundaries; is maintained by long-period systematic exchanges of potential and kinetic energies between the time-mean and transient fields of motion; and is accompanied by regular variations in the stability properties of the flow. Unlike the studies noted above, it is not our intention to carry out a complete parametric description of this phenomenon on the basis of many experiments; rather, we wish to discuss the kinematic and energetic character of a single EGCM vacillation cycle in the parametric neighborhood of its occurrence.

2. Description of the basic experiment

The numerical experiments discussed here were carried out with the flat-bottom two-layer quasi-geostrophic model described by Holland (1978). The vacillation cases we shall analyze (experiments V1–V9) are in fact very similar to one of the experiments described therein (experiment 1; hereafter H1). The reader is referred to that paper for a more complete discussion of the model and of experiment H1 results, as well as for better insight into how these experiments fit into the broader parametric study.

Following Holland (1978), the two-layer quasi-geostrophic equations can be written in nondimensional form as

$$\frac{\partial}{\partial t}\nabla^2\psi_1 = R_0 J(\nabla^2\psi_1, \psi_1) - \psi_{1x} - \delta_3 w_2 + E\nabla^4\psi_1 - \sin(\pi y/L), \quad (1)$$

$$\frac{\partial}{\partial t}\nabla^2\psi_3 = R_0 J(\nabla^2\psi_3, \psi_3) - \psi_{3x} + \delta_1 w_2 + E\nabla^4\psi_3, \quad (2)$$

$$\frac{\partial}{\partial t}(\psi_1 - \psi_3) = R_0 J(\psi_1 - \psi_3, \psi_2) - \gamma^2 w_2. \quad (3)$$

The five nondimensional parameters governing the flow are the Rossby number $R_0 = \pi\tau_0/(H_1\beta^2L^3)$, the ratio of the internal radius of deformation to the basin width $\gamma = (g'H_1H_3/f_0^2H)^{1/2}/L$, the Ekman number $E = A_m/\beta L^3$, and the layer depth ratios $\delta_1 = H_1/H$ and $\delta_3 = H_3/H$. Here $g' = g\nabla\rho/\rho$ is "reduced gravity," $f = f_0 + \beta y$ is the Coriolis parameter, H_1 and H_3 are the resting thicknesses of the upper and lower layers, $H = H_1 + H_3$ is the (constant) total depth, and A_m is a coefficient of lateral viscosity. The wind stress has the single gyre form $\tau = \tau_0 \cos(\pi y/L)$, where L is the lateral extent of the square basin. The ψ_i $(i = 1, 3)$ are the quasi-geostrophic streamfunctions with velocity components $(u_i, v_i) = (-\partial\psi_i/\partial y, \partial\psi_i/\partial x)$, J is the Jacobian operator, and w_2 is the vertical velocity at the interface. Three-dimensional length scales of interest

$$w_i = R_0^{1/2}L = (\pi\tau_0/H_1\beta^2L)^{1/2},$$

$$w_f = 2E^{1/3}L = 2(A_m/\beta)^{1/3},$$

$$r_d = \gamma L = (g'H_1H_3/Hf_0^2)^{1/2},$$

TABLE 1. The experiments discussed in this study, including experiment 1 described in Holland (1978). In all experiments, $H_1 = 1000$ m, $H_3 = 4000$ m, $L = 1000$ km, $\beta = 2 \times 10^{-11}$ m^{-1} s^{-1}, $g' = 0.02$ m s^{-2}. All values of the parameters are shown for H1 and V1; only those values that differ from V1 are shown for experiments V2–V9.

Experiment No.	τ_0 (10^{-4} m^2 s^{-2})	f_0 (10^{-5} s^{-1})	A_m (m^2 s^{-1})	R_0	γ^2	E	W_i (km)	W_m (km)	R_d (km)	Long-time scale eddies present
H1	1	8.3	330	7.9×10^{-4}	2.3×10^{-3}	1.6×10^{-5}	28.0	50.9	48.0	No
V1	1	7.3	330	7.9×10^{-4}	3.0×10^{-3}	1.6×10^{-5}	28.0	50.9	54.8	Yes
V2		7.8			2.6×10^{-3}				51.3	No
V3		6.8			3.5×10^{-3}				58.8	Yes
V4			260			1.3×10^{-5}		47.0		No
V5			400			2.0×10^{-5}		54.3		Yes
V6	1.2			9.4×10^{-4}			30.7			No
V7	0.8			6.3×10^{-4}			25.0			Yes
V8		6.3			4.0×10^{-3}				63.5	No
V9			500			2.5×10^{-5}		58.5		No

are respectively the width of a purely intertial western boundary current, the width of a purely frictional western boundary current, and the radius of deformation.

With the specification of impermeable free-slip lateral walls, Eqs. (1)–(3) are integrated in time, typically from a state of rest. For the experiments described below, a second-order finite-difference technique with grid spacing $\Delta x = \Delta y = 20$ km has been used (Holland, 1978). It is relevant to note, however, that the V1 vacillation cycle was originally observed in a (physically identical) two-layer quasi-geostrophic model which, however, used an entirely different (pseudospectral) solution technique (Haidvogel, 1976). There was no statistically significant difference between the finite-difference and pseudospectral models in any of the global diagnostic quantities discussed below (e.g., fast and slow eddy period, and energy transfers). It is unlikely, therefore, that the observed vacillation is computational in origin.

Experiment H1 and the central vacillation experiment V1 represent cases of two-layer quasi-geostrophic flow in a small free-slip basin driven by a steady wind stress of single-gyre form and retarded by lateral friction. Table 1 shows the relevant dimensional and nondimensional parameters for the experiments. Note that a limited nondimensional parameter study (experiments V2–V9) has been carried out with differing values of R_0, E and γ in order to delineate the parametric region where vacillation occurs. This aspect of the study will be discussed in the next section.

To illustrate the basic character of the vacillation phenomenon in experiment V1, we shall examine energy spectra, basin-averaged time series of kinetic and potential energies, and streamfunction maps for the slowly varying mean flow and the fast time-scale

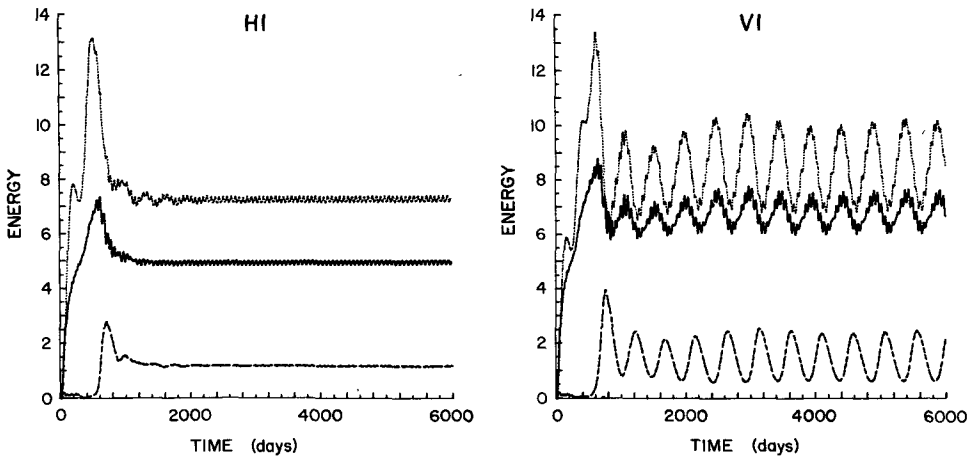

FIG. 1. The basin-averaged energies for experiments H1 and V1. The upper curves are potential energies; the middle curves, upper layer kinetic energies; and the lower curves, lower layer kinetic energies. Energy units are 10^6 ergs cm^{-2}.

eddy motion. To interpret this observed behavior, at least in a qualitative fashion, we will appeal to the results of linear stability analyses which suggest that the baroclinic energy conversion process driving the fast time scale (mesoscale) eddies undergoes a slow strengthening and weakening.

The globally averaged kinetic and potential energies as a function of time in experiments H1 and V1 are plotted in Fig. 1. Initiated from rest, both experiments are spun up until about day 500 at which time the onset of instability leads to a readjustment of energy between the potential (P) and kinetic (K_1, K_3) energies. Subsequently, both experiments settle into a regular oscillating equilibrium state. In experiment H1 only a "fast" time scale exists with a period of about 64 days. Experiment V1, however, displays variations on both a fast and slow time scale (60 and 480 day periods, respectively). The oscillations are very regular. Note (Table 1) that these experiments differ slightly only in their respective values of the radii of deformation, yet this modest difference leads to quite different physical behavior.

Local kinetic energy spectra taken at a point in

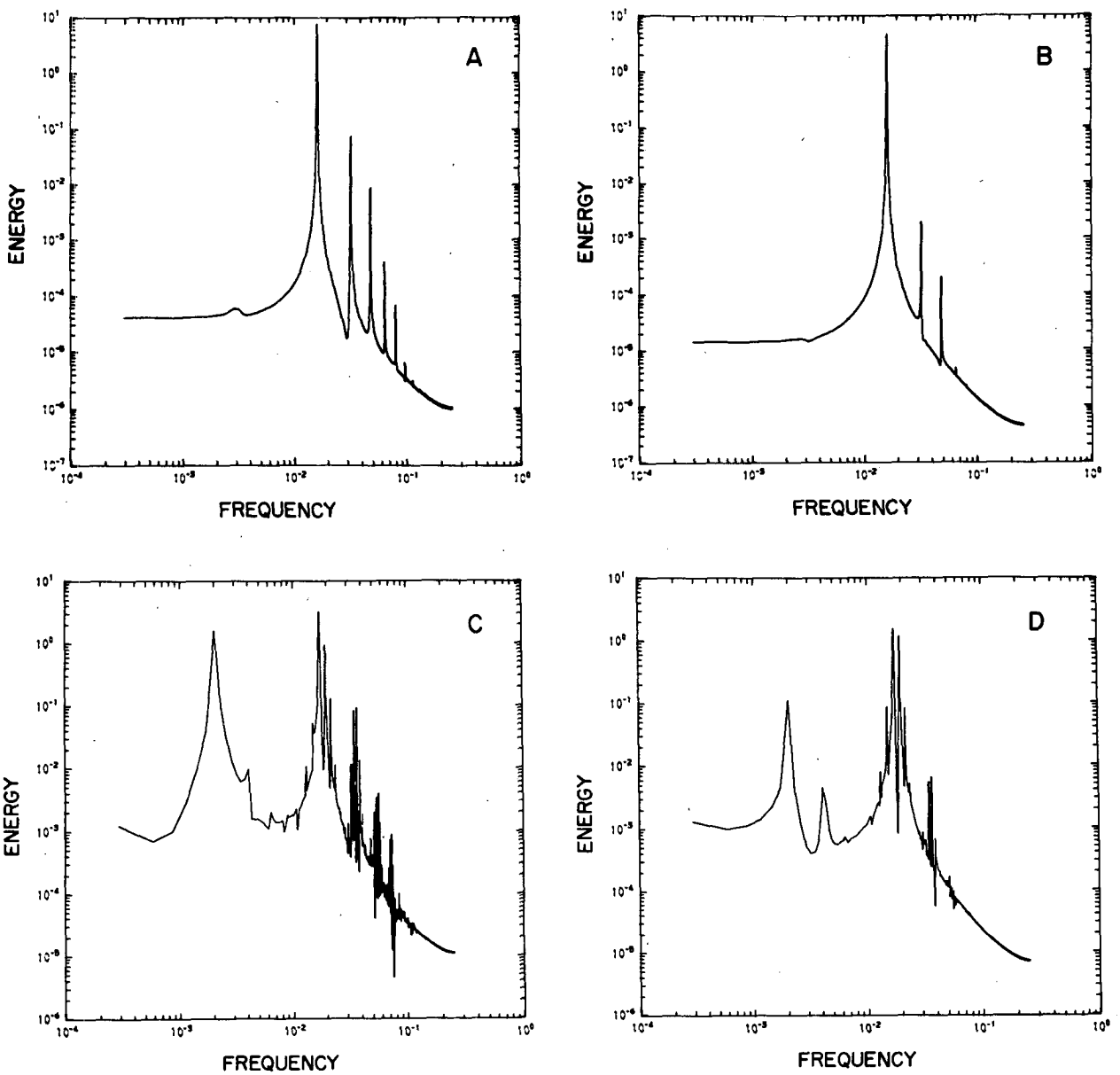

FIG. 2. Energy spectra from a single location in experiments H1 and V1. Units are days^{-1} (abscissa) and m^2 s^{-2} (ordinate). By our convention, the period of the motion equals (frequency)$^{-1}$. The spectra are: (A) H1, upper layer; (B) H1, lower layer; (C) V1, upper layer; and (D) V1, lower layer.

the north-central part of the basin are consistent with these globally integrated statistics. Figs. 2a and 2b show the kinetic energy spectra for the upper and lower layers of experiment H1; (2c and 2d) show the corresponding spectra for V1. Observe in V1 the very large peak at about 480 days, completely missing in H1. Additionally, there is a very large spectral gap between the frequency peaks in V1 which will allow us to separate these components rather cleanly into fast (periods < 150 days) and slow (periods > 150 days) time scales. In other, more nonlinear experiments—e.g., experiments 3 and 5 in Holland (1978)—eddy energy occupies a much broader continuum; there is no clear separation of fast and slow time scales of motion.

Using a very long time series of streamfunction maps obtained during the statistical equilibrium phase of V1, it is possible to determine the long-time-mean flow, its slow variation and the superimposed fast (mesoscale) oscillation. To do so, we define the long-term mean flow as

$$\bar{\psi}_i = T^{-1} \int_{T_1}^{T_1+T} \psi_i dt, \quad i = 1, 3,$$

where the initial time (T_1) and averaging interval (T) are 1200 and 5240 days, respectively. To recover the slow variation of the mean flow, we form a running average to eliminate the fast time-scale eddy component

$$\psi_{is}(\tau) = \frac{1}{2}(\delta\tau)^{-1} \int_{\tau-\delta\tau}^{\tau+\delta\tau} (\psi_i - \bar{\psi}_i) dt, \quad i = 1, 3,$$

where we let $\delta\tau = 30$ days. Finally, the fast eddy field

$$\psi_{if}(t) = \psi_i(t) - \bar{\psi}_i - \psi_{is}(t), \quad i = 1, 3.$$

This decomposition produces a simple description of the "slowly varying mean flow," $\bar{\psi}_i + \psi_{is}$. We note that when this procedure is applied to experiment H1, the amplitudes of ψ_{is} are very small in comparison to ψ_{if}, whereas in V1 they are of comparable magnitude.

Fig. 3 shows the mean flows and Fig. 4 the (mean + slow) oscillation defined in this way. The mean flows are similar in character to the means of experiment H1. Both are characterized by western and northern boundary currents, westward return flow in the upper layer and a pair of recirculating gyres in the deep ocean. The slow oscillation (Fig. 4) can weaken or strengthen the long-term mean flow by ~20% in the upper layer and 50–100% in the lower layer. The main center of action is the northwest corner of the basin, that is, the region of inertial recirculation.

An energetic description of the interaction between the fast eddies and the slowly varying mean can be achieved by constructing energy box diagrams (Holland, 1978) for various subperiods of the slow variation. We have calculated the average energy and energy fluxes over successive 60-day periods during the vacillation cycle by choosing the eddy signal in each subinterval to be the deviation from the local 60-day mean flow. The slow variation in energetic transfer rates suggests a slow variation in the instability process giving rise to the fast eddies. Figs. 5 and 6 show the results of this construction.

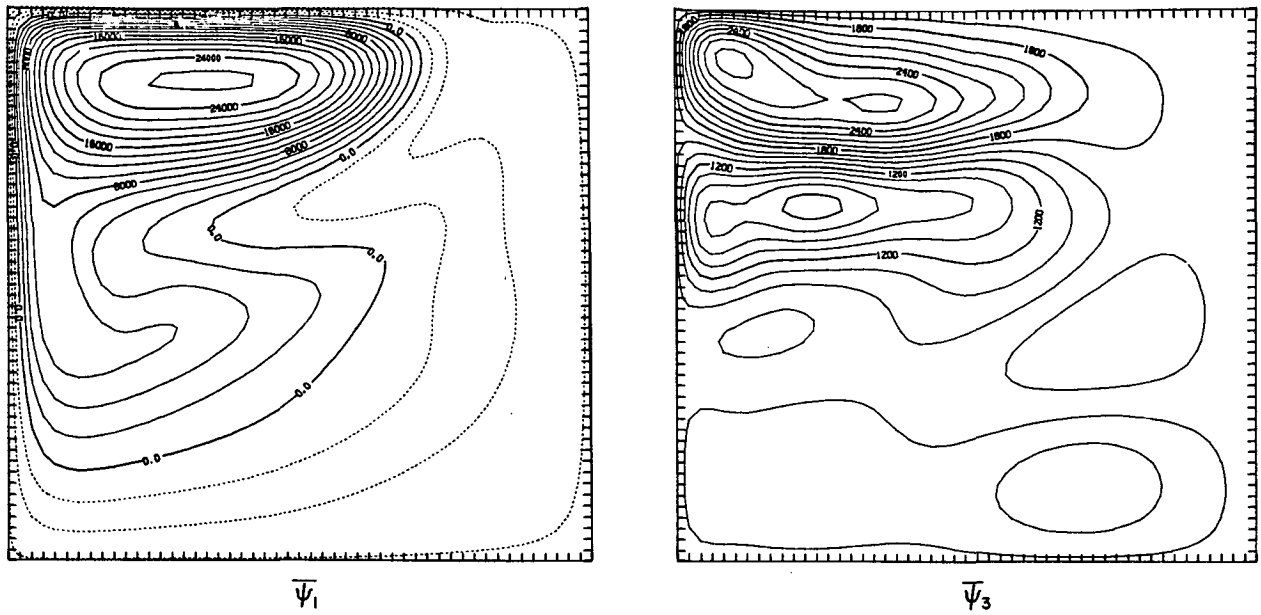

FIG. 3. Quasi-geostrophic streamfunctions for the long-term mean flows $\bar{\psi}_i$ of experiment V1. The contour intervals are 2000 m^2 s^{-1} ($\bar{\psi}_1$) and 150 m^2 s^{-1} ($\bar{\psi}_2$).

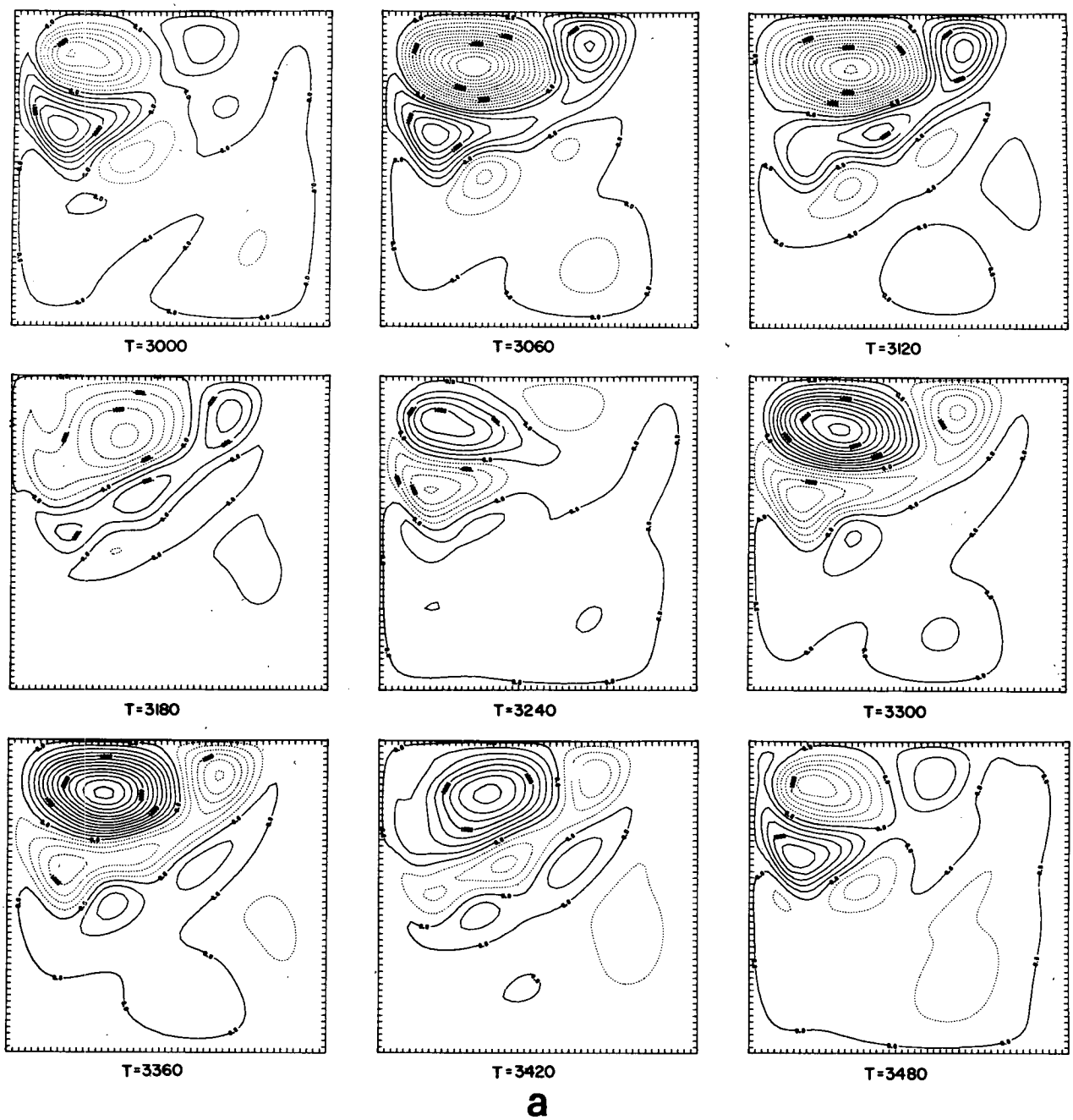

FIG. 4. The slowly varying components of the quasi-geostrophic streamfunctions (ψ_{is}) for experiment V1. The maps show one oscillation of the slow time scale (480 days) at 60-day intervals. (a) Upper layer (contour interval = 4000 m^2 s^{-1}); (b) lower layer (contour interval = 100 m^2 s^{-1}).

Note first that the energy input by the wind varies by only 6% over the course of the slow oscillation. The net energy flow from the slowly varying mean to the fast eddy field, however, changes from 0.09 ergs cm^{-2} s^{-1} at its minimum (180–240 days) to 0.69 erg cm^{-2} s^{-1} at its maximum (420–480 days) half a (long) period later. The baroclinic energy conversion varies by a factor of 6 over the 480-day period of the slow oscillation. A careful examination of the time sequence of Fig. 5 shows that during half of the 480 period the eddies are losing energy to friction faster than they are gaining it via baroclinic instability processes (and to a lesser extent barotropic transfers); consequently, their net energy decreases (Fig. 6). During the other half period, the net energy flow into the eddies due to instability

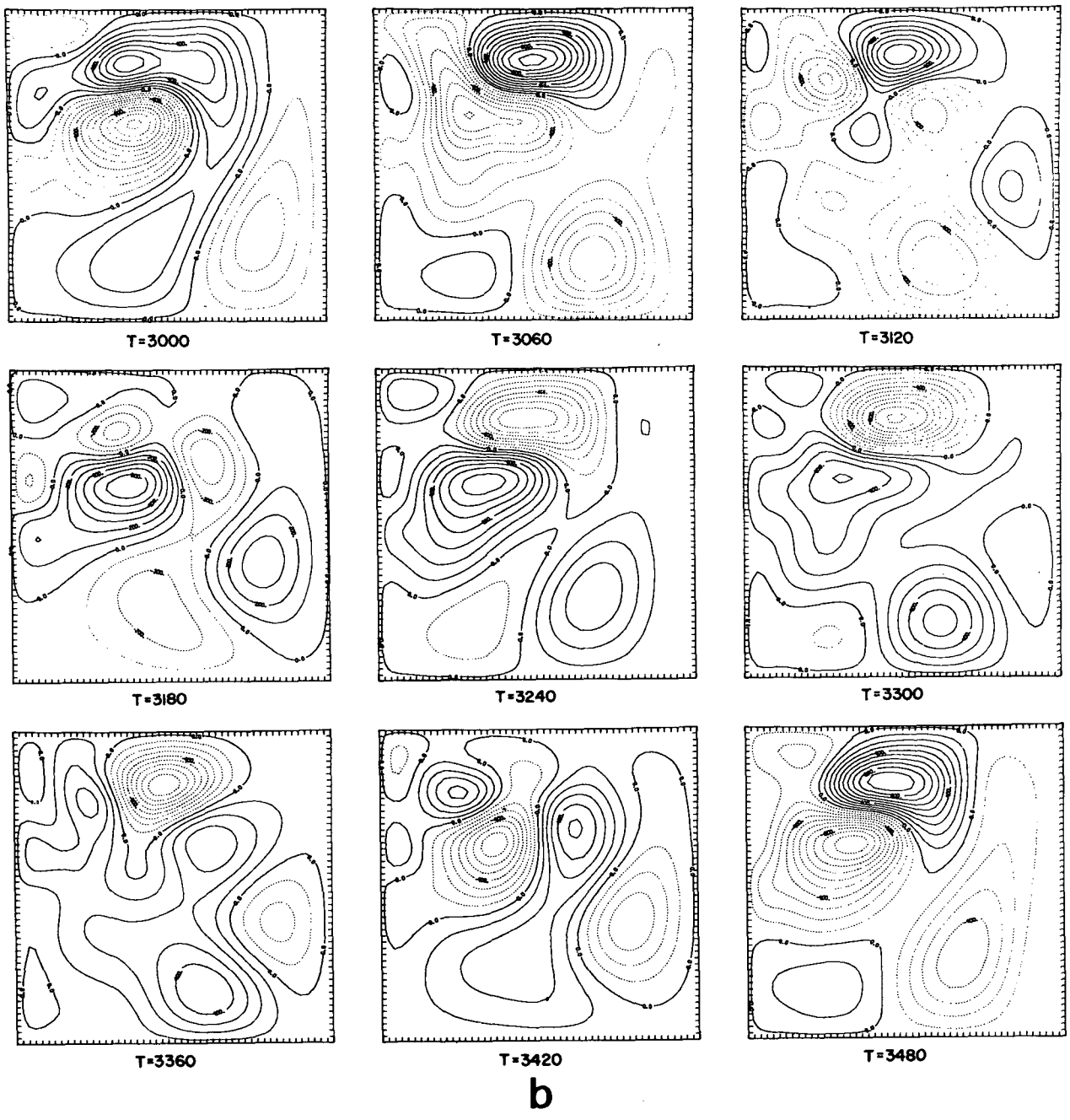

FIG. 4. (*Continued*)

exceeds dissipation. The mean energy components also vary over this time scale as energy input by the wind is greater than (less than) the net loss due to dissipation and energy transfer to the eddy field. Fig. 6 shows the variation in time of these energy components.

In an earlier analysis of eddy-resolving general circulation experiments, Haidvogel and Holland (1978) found it possible to understand some of the kinematic and dynamic properties of the eddying circulations using linear stability theory. (Particular success was achieved in this application of linear theory for less turbulent simulations such as H1.) Here we adopt the identical approach, examining the slowly varying flow for its stability properties. Taking a north-south section across the long-time mean flows (Fig. 3) at a longitude 400 km east of the western boundary, application of the two-dimen-

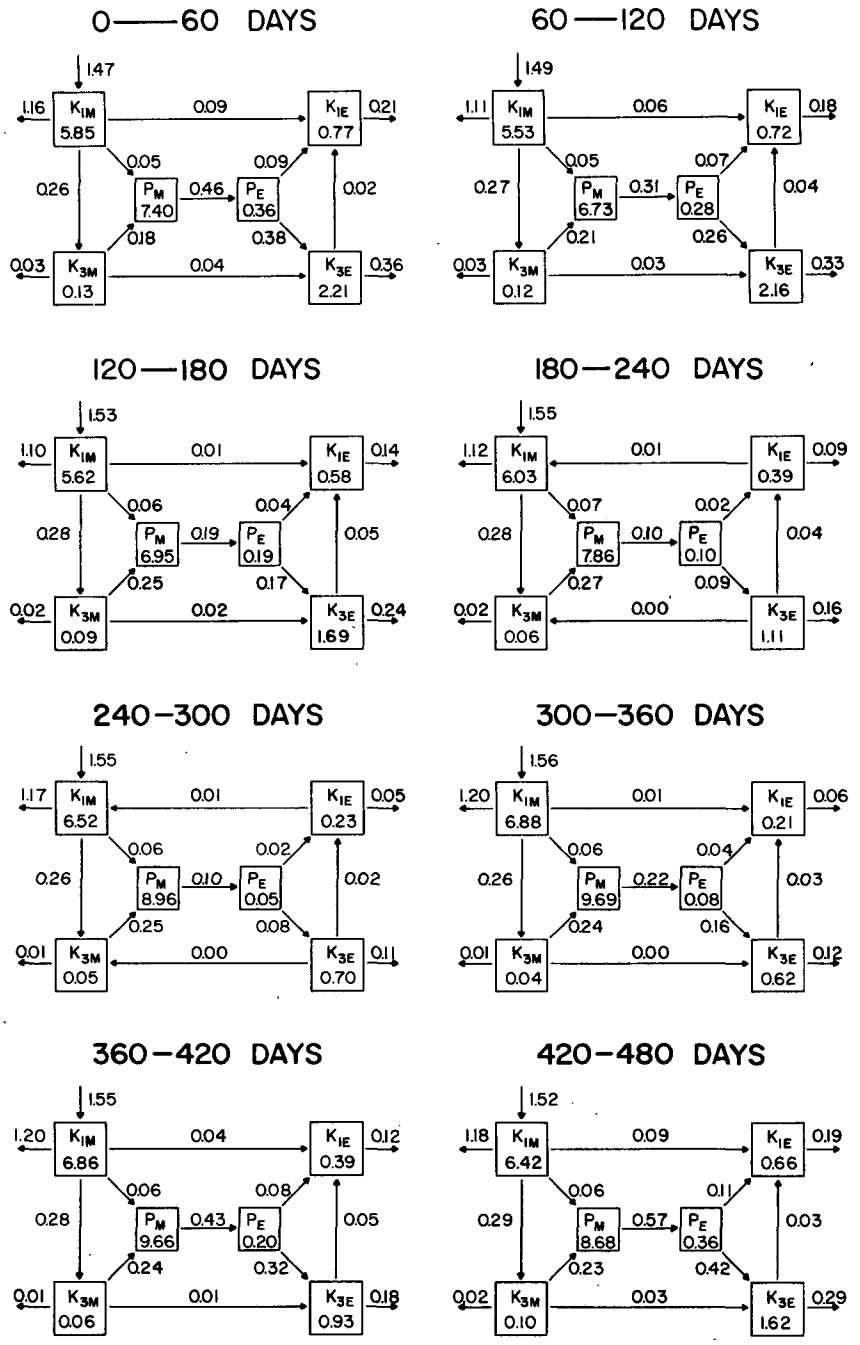

FIG. 5. Energy budget based upon "slowly varying" mean flows, $\psi_i + \psi_{is}$, and rapidly varying eddies [see Holland (1978) for definitions of energy and energy fluxes]. The box energy diagrams show energy levels and energy flux rates for various sub-periods of the slow oscillation. Energy units (within boxes) are 10^6 ergs cm^{-2}; energy flux units (arrows) are ergs cm^{-2} s^{-1}.

sional stability analysis described by Haidvogel and Holland (1978) gives the stability curve marked b in Fig. 7. The maximum growth rate of the unstable wave (e-folding time of 62.5 days) occurs at a wavelength of ~400 km. Now taking the slowly varying mean flows—the means of Fig. 3 plus the slow components shown in Fig. 4—first at T = 3120 days, where the slow oscillation serves to weaken the upper flow, then at T = 3360 days, where the slow oscillation strengthens the upper layer flow, we find the growth rate results also shown in Figs. 7a and 7c. For the weaker upper layer flow (Fig. 7a) the e-fold-

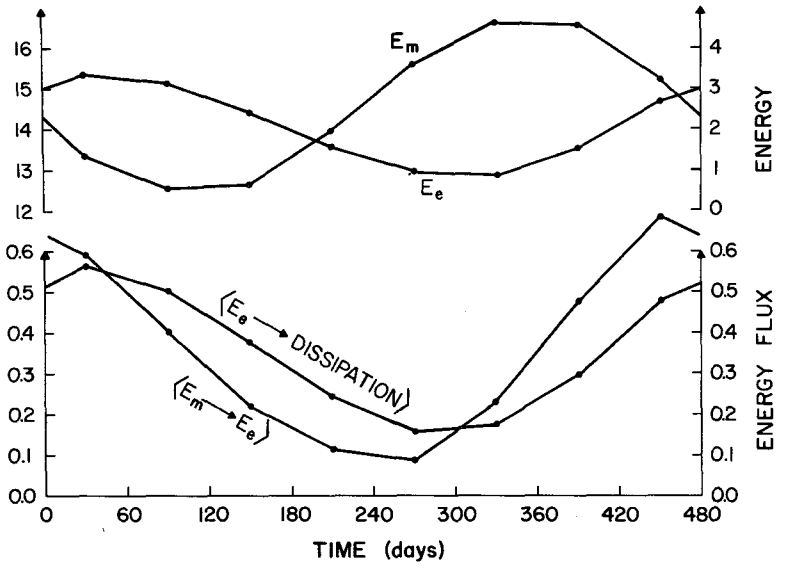

FIG. 6. Upper panel: The slow oscillation in mean and eddy energies ($E = P + K_1 + K_2$). The left-hand scale is for mean energy and the right-hand scale is for eddy energy. Units are 10^6 ergs cm^{-2}. Lower panel: The slow oscillation in energy flux to the eddies $\langle E_m \rightarrow E_e \rangle$ is the net energy transfer into the eddy field from the mean by both baroclinic and barotropic conversion processes. $\langle E_e \rightarrow$ dissipation$\rangle$ is the net energy loss due to dissipation. The units are ergs cm^{-2} s^{-1}.

ing time is 145 days, corresponding to a much weaker instability; for the stronger upper layer flow (Fig. 7c), the e-folding time is reduced to 41 days, reflecting increased instability. These linear stability considerations reinforce the qualitative picture obtained by examining the slowly varying energetics—i.e., that the rate of energy transfer from slowly varying mean to eddies is describable as a slow vacillation in the baroclinic instability process in which growth of the eddies at the expense of the mean is followed by replacement of mean energy by the wind and decay of eddy energy due to dissipation.

3. A limited parameter study

To determine the breadth of the vacillation phenomenon in parameter space, eight additional experiments (V2–V9) were carried out (Table 1). These experiments encompassed systematic variations away from the V1 values of γ^2, R_0 and E. Experiments V2, V3 and V8 had values of $\gamma^2(f_0)$ different from the H1 and V1 values; vacillation occurs only for $(3.0 \times 10^{-3} \leqslant \gamma^2 \leqslant 3.5 \times 10^{-3})$. Experiments V6 and V7 examined changing R_0; vacillation occurs at considerably reduced amplitude for slightly smaller R_0 (6.3×10^{-4}), but is absent at larger R_0 (9.4×10^{-4}). Finally, experiments V4, V5 and V9 show vacillation to persist for a small fractional change in E (V5; $E = 2.0 \times 10^{-5}$) but to be absent for both larger and smaller values of the Ekman number (2.5×10^{-5}, 1.3×10^{-5}, respectively). Having approximately bracketed the vacillation in parameter space, we find it to be restricted to a rather narrow range of values of the basic parameters. These values are, however, in a geophysically interesting range.

We can most usefully summarize the results of experiments V2–V9 by showing the time dependence of the basin-averaged kinetic and potential energies for each experiment (Fig. 8), which can be compared with those for H1 and V1 (Fig. 1).

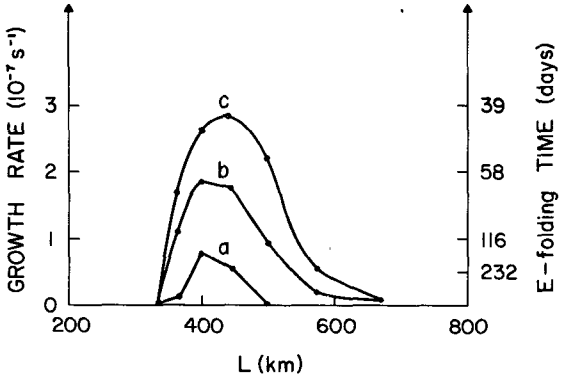

FIG. 7. Growth rates of the most unstable wave as a function of wavelength for three possible north-south sections of mean flow [see Haidvogel and Holland (1978) for a discussion of the linear stability analysis]: (a) the mean flow of Fig. 3 plus the slowly varying flow of Fig. 4 at $T = 3120$; (b) the mean flow of Fig. 3 alone; (c) the mean flow of Fig. 3 plus the slowly varying flow of Fig. 4 at $T = 3360$. The north–south section is taken at a longitude 400 km east of the western boundary.

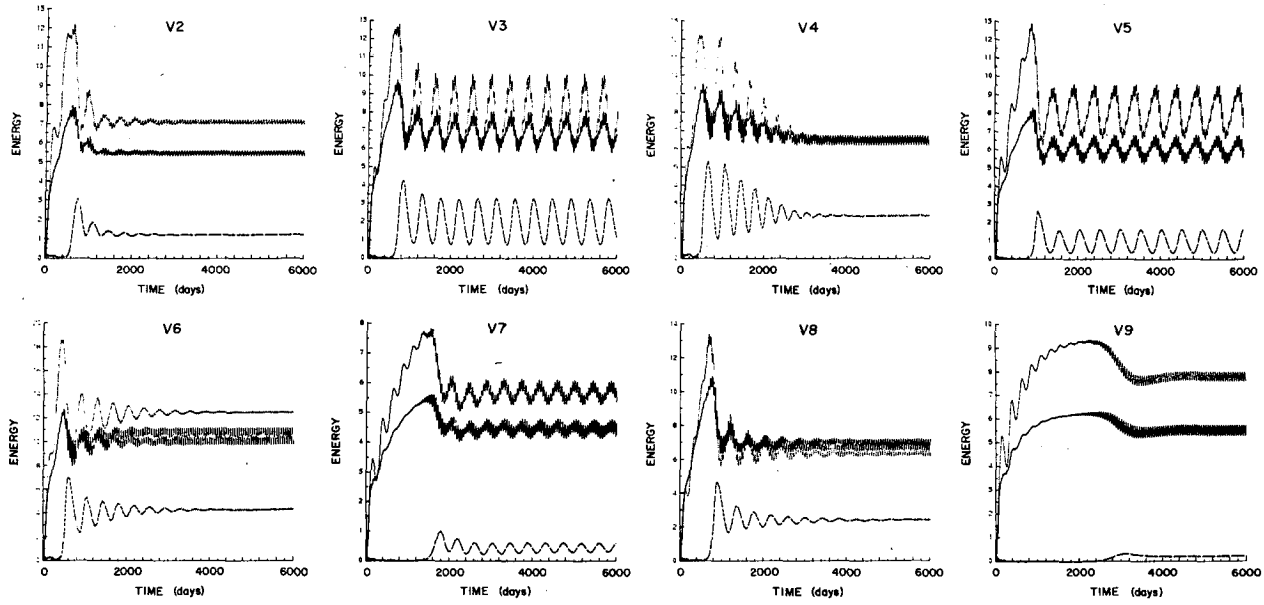

FIG. 8. The time-dependent behavior of the basin-averaged energies (10^6 ergs cm^{-1}) for the spinup of the various experiments. Note that all experiments have a fast eddy time scale (~60 days) but only V3, V5 and V7 have a slow time scale vacillation (~480-day period in all cases).

a. γ^2 variation

Note first that increasing γ^2 from its V1 value (experiment V2) results in a disappearance of the vacillation (Fig. 8). There is an initial tendency for a vacillation to develop just following the spin-up phase but it does not persist; instead, it decays away in ~1500 days, leaving only the fast time-scale oscillation. Reducing γ^2 (experiment V3) leads to a vigorous vacillation of even larger amplitude than experiment V1. Reducing γ^2 further (experiment V8), however, leads to the vacillation just dying away (but very slowly, over ~3000 days). Experiment V8 appears to be very near to marginal stability as far as the production of the long-time scale is concerned.

b. R_0 variation

Comparing experiments V6 and V7 with V1, we find that the larger R_0 value (V6) leads to an equilibrium with no vacillation while the smaller R_0 value (V7) leads to a reduced amplitude of the vacillation. Presumably the vacillation would not survive at a slightly smaller R_0 value. Note the change in the mean energy levels for these experiments as the strength of the forcing is successively decreased (V6 → V1 → V7).

c. E variation

Experiments V4, V5 and V9 examine the results of varying the strength of friction, relative to V1. Smaller friction (V4, Fig. 8) ultimately supresses the vacillation although initial large-amplitude long-time scale variations are apparent. At slightly larger friction (V5), the behavior is quite similar to V1, with persistent large-amplitude vacillation occurring in the final statistical equilibrium. However, at even larger friction (V9), vacillation again disappears; only weak mesoscale (fast time scale) eddies are present.

Results from the vacillating flows in V1, V3, V5 and V7 are further summarized (Fig. 9) in terms of the slow change in total energy transfer to the eddy field. Note that the vacillation time scales are nearly constant for all these cases (~480 days). This is true as well for the fast time scale (~60 days). The amplitudes of the slow time-scale variation over a wide range with V3 being the most vigorous and V7 showing only a relatively small vacillation cycle. All experiments indicate a positive net energy transfer to the eddy field at all phases of the slow cycle, but they all approach closely to zero at their respective minima. Thus, while at the maximum, the energy transfers from mean field to eddy motions may be vigorous, there seems always to exist one phase of the vacillation cycle in which the basic baroclinic instability that gives rise to the fast time scale eddies is very nearly "turned off."

We note in passing that other parameters and modeling assumptions have implicitly been held fixed in this brief parameter study. Among the most important of these are the assumed initial conditions (a state of rest), and the level of surface friction (here assumed negligible). Although nonlinear equilibration in weakly turbulent systems such as these

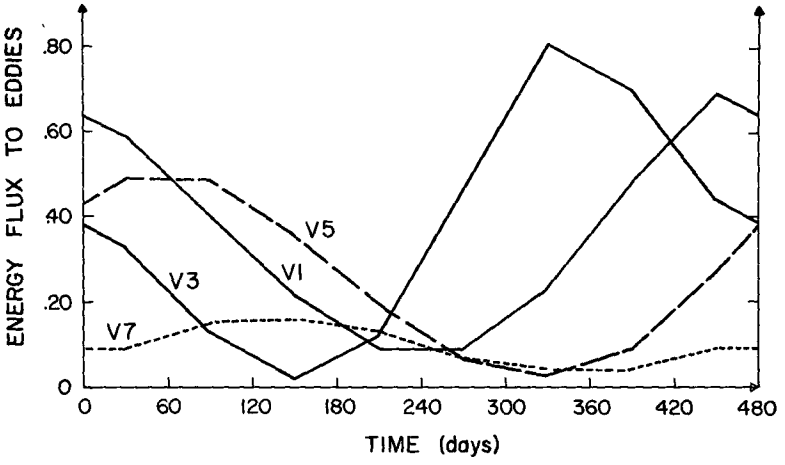

FIG. 9. The slow variation in total energy flux to the eddy field for the four experiments showing vacillation (energy flux units are ergs cm^{-1} s^{-1}).

can be sensitive to initial conditions, we know of no documented instance of such EGCM sensitivity. In one of several previous instances in which a direct comparison was made, the equilibrium results of experiment H1 were not observed to change if the system was not initially at rest. However, we have not performed a separate initial condition sensitivity study in the context of these vacillation experiments; therefore, we cannot entirely rule out the importance of initial conditions. Likewise, we have ignored the effects of bottom friction in these studies. We have done so to limit the complexity and expense of the parametric study, and because the vacillation was first observed in the absence of such effects. Given the narrowness of the parameter range in which the vacillation seems to occur, we suspect that the V1 vacillation cycle would disappear if rather weak bottom friction were added. However, this speculation—and the relation of these results to the earlier models mentioned in the Introduction—has yet to be explored.

4. Discussion

It has not been our intention in this note to elucidate the physical *causes* for the vacillation cycle observed to occur in this eddy-resolving ocean circulation model. The complexity of the highly inhomogeneous eddying circulations in these EGCM experiments would make this a formidable task. Instead, we have simply *described* the cycle, related it to certain long time-scale changes in the energetics of the system, and traced out the limited region in parameter space in which the vacillation phenomenon occurs.

It seems likely to us that this behavior is relatively simple in these experiments because friction is fairly strong and the flow field only weakly unstable. In other experiments, in which lateral friction is small (Holland, 1978), the flow is very much more "turbulent" and the energy spectrum very much broader band. It may be that similar processes may yet operate to produce energy at the longer time scales in these calculations; however, very much more sensitive diagnostic techniques than those presently available for EGCM analysis would be needed to assess this possibility. Indeed, much simpler models of these processes may be required to understand such transfers in the frequency domain. It is interesting to speculate that a limited-component model—similar to those so effectively studied by Lorenz (1963), Hart (1976), and Pedlosky (1972)—could be used to investigate the underlying dynamics involved in the V1 vacillation cycle.

Although the importance of multiyear vacillation in the ocean is not known, it seems likely that long time-scale oceanic variability will be coupled at least in part to variations in the earth's climate. Therefore, it will be important in future to investigate the mechanisms that can lead to relatively energetic, long time-scale variability in the oceans and, ultimately, to deduce whether they are internal (inherently oceanic mechanisms) or external (associated with forcing of the ocean by the atmosphere).

Acknowledgments. The work of one of the authors (DBH) has been supported by the National Science Foundation through Grant OCE78-25700 to the Woods Hole Oceanographic Institution. Computational resources were provided by the National Center for Atmospheric Research, which is also funded by the National Science Foundation. This paper is Contribution 4741 of the Woods Hole Oceanographic Institution and 154 of the POLYMODE program.

REFERENCES

Haidvogel, D. B., 1976: The sensitivity and predictability of mesoscale eddies in an idealized ocean model. Ph.D. dissertation, MIT and WHOI, 245 pp.

——, and W. R. Holland, 1978: The stability of ocean currents in eddy-resolving general circulation models. *J. Phys. Oceanogr.*, **8**, 393–413.

Hart, J. E., 1972: A laboratory study of baroclinic instability. *Geophys. Fluid Dyn.*, **3**, 181–209.

——, 1976: The modulation of an unstable baroclinic wave field. *J. Atmos. Sci.*, **33**, 1874–1889.

Hide, R., 1953: Some experiments on thermal convection in a rotating liquid. *Quart. J. Roy. Meteor. Soc.*, **79**, 161.

Holland, W. R., 1978: The role of mesoscale eddies in the general circulation of ocean—numerical experiments using a wind-driven quasigeostrophic model. *J. Phys. Oceanogr.*, **8**, 363–392.

Lorenz, E. N., 1963: The mechanics of vacillation. *J. Atmos. Sci.*, **20**, 448–464.

Pedlosky, J., 1972: Limit cycles and unstable baroclinic waves. *J. Atmos. Sci.*, **29**, 53–63.

Pfeffer, R., G. Buzyna and W. W. Fowlis, 1974: Synoptic features and energetics of wave-amplitude vacillation in a rotating, differentially-heated fluid. *J. Atmos. Sci.*, **31**, 622–645.

Webster, P. J., and J. L. Keller, 1975: Atmospheric variations: Vacillations and index cycles. *J. Atmos. Sci.*, **32**, 1283–1300.

Addendum to the Dynamics of Oceanic Fronts. Part I: The Gulf Stream

TIMOTHY W. KAO

Department of Civil Engineering, The Catholic University of America, Washington, DC 20064

9 October 1980 and 1 December 1980

ABSTRACT

The nature of the balance of forces in the downstream direction is discussed. It is shown that the ageostrophic cross-stream flow is in advective equilibrium in which the Coriolis force is balanced by the nonlinear inertia force.

In a recent paper, Kao (1980), a frontal model of the Gulf Stream was presented. It was shown that in the quasi-steady state, geostrophic balance was achieved in the cross-stream direction. The balance of forces in the downstream direction was not discussed. This note is to fill this omission. Simply stated, the balance of forces in the downstream direction is between the Coriolis force due to the ageostrophic cross-front flow and the inertial force of the nonlinear advection terms, i.e., in the quasi-steady state in which the front is stationary (except for a small inertial period oscillation),

$$\underset{\text{A}}{\frac{\partial}{\partial \xi}[(\tilde{u}-\tilde{u}_f)\tilde{v}]} + \underset{\text{B}}{\frac{\partial}{\partial \eta}(\tilde{w}\tilde{v})} + \underset{\text{C}}{(\tilde{u}-\tilde{u}_f)} = 0, \quad (1)$$

to order E times the order of magnitude of A, B or C. For the definition of symbols see Kao, 1980. Terms A and B represent the rate of change of the downstream momentum due to horizontal advection in the cross-stream direction and due to vertical advection, respectively. Term C represents the Coriolis force in the downstream direction. The typical magnitudes of terms A, B and C in Eq. (1) are listed in Table 1 at different depths in the water column at two different cross-stream locations $\xi_{\tilde{a}} = -0.52$ and $\xi_{\tilde{a}} = -0.33$ which are both in the warm pool (or Sargasso Sea) side of the frontal region (see Fig. 4 of Kao). Column D in the table represents the sum A + B + C. It is seen that the stated balance of Eq. (1) is indeed achieved throughout the depth. (Note that $E = 0.025$). In dimensional units, if the reference velocity U_d is 1 m s^{-1} in a typical Gulf Stream case, and f is 10^{-4} s^{-1}, then a value of 1 for the entries under A, B, C or D represents 10^{-2} dyn cm^{-3}. It

TABLE 1. Values of horizontal advection A, vertical advection B and the Coriolis term C in the downstream momentum balance, for the Gulf Stream frontal model with $E = 0.025$. Values are given at various depths for two different horizontal locations.

η_2	A	B	C	D = A + B + C
$\xi_{\tilde{a}} = -0.52$				
0.04	0.0870	−0.1632	0.0748	−0.0014
0.26	0.1368	−0.1530	0.0187	0.0025
0.48	0.0083	0.0492	−0.0557	0.0018
0.71	−0.1330	0.1622	−0.0324	−0.0032
0.93	−0.0627	0.0648	−0.0014	0.0007
1.15	−0.0043	−0.0006	0.0098	0.0049
$\xi_{\tilde{a}} = -0.33$				
0.04	0.0838	−0.2576	0.1764	0.0026
0.26	0.0949	−0.1853	0.0887	−0.0017
0.48	−0.0250	0.0992	−0.0768	−0.0026
0.71	−0.0099	0.0960	−0.0855	0.0006
0.93	−0.0291	0.0789	−0.0463	0.0035
1.15	−0.0355	0.0460	−0.0092	0.0013

0022-3670/81/040568-02$04.50